

# Co-existence of Terrestrial and Non-Terrestrial Networks in S-band

Niloofer Okati , Andre Noll Barreto, Luis Uzeda Garcia , and Jeroen Wigard

**Abstract**—Co-existence of terrestrial and non-terrestrial networks (NTN) is foreseen as an important component to fulfill the global coverage promised for sixth-generation (6G) of cellular networks. Due to ever rising spectrum demand, using dedicated frequency bands for terrestrial network (TN) and NTN may not be feasible. As a result, certain S-band frequency bands allocated by radio regulations to NTN networks are overlapping with those already utilized by cellular TN, leading to significant performance degradation due to the potential co-channel interference. Early simulation-based studies on different co-existence scenarios failed to offer a comprehensive and insightful understanding of these networks' overall performance. Besides, the complexity of a brute force performance evaluation increases exponentially with the number of nodes and their possible combinations in the network. In this paper, we utilize stochastic geometry to analytically derive the performance of TN-NTN integrated networks in terms of the probability of coverage and average achievable data rate for two co-existence scenarios. From the numerical results, it can be observed that, depending on the network parameters, TN and NTN users' distributions, and traffic load, one co-existence case may outperform the other, resulting in optimal performance of the integrated network. The analytical results presented herein pave the way for designing state-of-the-art methods for spectrum sharing between TN and NTN and optimizing the integrated network performance.

**Index Terms**—Non-terrestrial networks (NTN), Low Earth orbit (LEO) Internet constellations, interference, co-existence, stochastic geometry, coverage probability, data rate, spectrum sharing

## I. INTRODUCTION

Non-terrestrial networks (NTN) is foreseen as an integral part of sixth-generation (6G) cellular networks to fulfill the requirements on expanding coverage and connectivity in remote and underserved areas [1]. NTN encompass different types of networks communicating through the sky (air or space), including satellite-based networks, high-altitude platform systems (HAPSs), and unmanned aerial vehicles (UAVs). During the recent years, due to the significant reduction in the launch costs of satellites and increased demand for global broadband connectivity, low Earth orbit (LEO) satellites outpaced other types of NTN in commercialization, leading to several initiatives such as Starlink, OneWeb, AST SpaceMobile and Project Kuiper [2].

The integration of NTN technology into terrestrial networks (TN) for the next-generation communication systems, such as 6G, holds great potential for revolutionizing global connectivity [3], by complementing terrestrial infrastructure and extending connectivity to remote areas, such as rural regions, maritime environments, and disaster-stricken locations. However, the successful deployment and operation of NTN

systems face several challenges, one of which is the scarcity of spectrum resources. The limited availability of suitable frequency bands may impose that NTN and TN systems operate in shared frequency bands, which will inevitably cause interference between both systems. To address this limitation, it becomes imperative to explore mechanisms for sharing and co-existence between NTN and TN, while ensuring efficient spectrum utilization and minimizing interference.

Due to the massive number of nodes and the large number of possible combinations, Monte Carlo simulation-based performance evaluation of the TN-NTN integrated network is computationally demanding. In this paper, to evaluate the interference effect of an NTN network on the performance of a TN network, we utilized stochastic geometry as a powerful mathematical framework which has a rich history in modeling and analyzing of wireless networks [4]. Stochastic geometry enables obtaining analytical tractable derivations on the performance of the integrated network using the spatial distribution of network elements, e.g., base stations (BSs) and user equipments (UEs). The analysis provides several insights into the impact of different network parameters, such as the density of TN BSs, NTN BSs' altitudes, inter-site distance (ISD), the number of UEs, and the minimum separation distance between the users of each network, on the network's performance. Obviously, such results will pave the way for design of different co-existence mechanisms and spectrum sharing policies required to enable seamless operation of NTN and TN systems.

### A. Related Works

The integration of NTN and TN is proposed and investigated in many prior arts in the literature. In [5], the performance of fifth-generation (5G) TN is compared with that of a LEO satellite network using an experimental setup in a suburban environment, in terms of latency and throughput. It was demonstrated that multi-connectivity between both networks can provide coverage seamlessly for low-latency and high-reliability requiring services. Co-existence and spectrum sharing studies have received significant attention in the International Telecommunication Union (ITU) agenda. For instance, a simulation tool that analyses the aggregate interference between 5G TN and other networks following ITU recommendations was presented in [6]. It was used, for instance, in [7] to investigate co-existence of 5G and HAPS.

Several methods for spectrum sharing between TN and LEO satellites have been suggested in the literature. In [8], a methodology using open radio-access network (ORAN) was

proposed, in which interference is reported by the ORAN terrestrial networks to the satellite service provider. In [9], a simulation-based study for spectrum allocation between TN and NTN was developed to mitigate the co-channel interference to the NTN link. An experimental-based study on spectrum sharing between TN and a LEO satellite network was presented in [10], targeting as minimizing the interference from satellites at the TN users. Cognitive radio approaches for co-existence of satellites and TN cellular networks over the same frequency bands have been studied in [11], [12], targeting at better exploitation of frequencies that are not used by the terrestrial network. An overview of the integration of both geostationary earth orbit (GEO) and LEO satellites with 5G systems, focusing on enhanced mobile broadband (eMBB) and narrowband-IoT (NB-IoT) was presented in [13].

Stochastic geometry is a mathematical tool that finds extensive application across various scientific disciplines including wireless communication. Its utilization in the analysis of wireless networks dates back to 1961 to investigate the connectivity of large wireless networks with huge number of nodes [14]. Stochastic geometry is utilized for system level performance analysis of large wireless networks to avoid massive time consuming Monte Carlo simulations. Using stochastic geometry, the performance of the network is obtained by taking the averages over different realization of nodes in a network [4]. Averages can be computed over a large number of nodes' locations or several network realizations, for different metrics of interest, e.g., the probability of coverage and the average achievable rate. More particularly, the nodes' locations are modeled as a point process which captures the characteristics of their distribution, e.g., their density and the relative distances between them.

Stochastic geometry has found extensive application in the analysis of planar two-dimensional networks including heterogeneous [15]–[19], cognitive [20], [21], ad hoc [22]–[25], and vehicular [26], [27] networks. A comprehensive literature survey on utilization of stochastic geometry for modeling multi-tier and cognitive cellular networks has been provided in [18]. A taxonomy is founded on three key criteria: the type of network under consideration, the point process employed for modeling, and the network performance characterization techniques. The coverage and rate are tractably derived through modeling the BSs as a homogeneous PPP in [28] which is known as one of the seminal works on the utilization of stochastic geometry for performance analysis of a terrestrial cellular. The model shows the optimistic results of the conventional grid models while the stochastic model provides a lower band on the network performance.

The utilization of stochastic geometry for analyzing three-dimensional networks has been also compelling [29]–[31]. The tool was used to study different scenarios such as BSs being located on both ground and rooftops in highly crowded urban areas, UAV swarming, and massive satellite networks. Two spectrum sharing techniques, i.e., underlay and overlay, to share the spectrum between UAV-to-UAV and BS-to-UAV transceivers are analyzed in [32] by modeling both UAVs and BSs as homogeneous PPPs. The impact of interference from TN BSs on the primary users of a multi-beam geostationary

satellite when both networks share the same spectrum resources is investigated in [33]. Using the tools from stochastic geometry, authors analyzed two performance metrics of outage probability and area spectral efficiency under three secondary transmission schemes by modeling the satellite users and BSs as two independent point processes.

The application of stochastic geometry has been also extended for performance analysis of massive low Earth orbit constellations, by modeling the satellites as a binomial point process (BPP) [34]–[37] or a nonhomogeneous Poisson point process (NPPP) [38], [39] on a spherical shell which facilitates the utilization of the tools from stochastic geometry. In fact, a point process represents different realizations of satellites over the time caused by the motion of satellites on the orbits. Verification of the exact analytical derivations from the stochastic modeling with the actual simulated constellations represents a fair accuracy of such modeling. In [40], the coverage and rate of a noise-limited scenario is studied using stochastic geometry when the user is associated with a satellite which provides the highest signal-to-noise (SNR). Such association, compared to the simplistic case of associating the user with the nearest satellites, includes the effect of shadowing caused by the user's surrounding objects. The performance of multi-altitude LEO constellations when satellites are distributed on several orbital shells is studied in [36], [41].

In this paper, we study the coverage probability and average data rate of a primary TN network which shares the same spectrum resources with a secondary LEO network in S-band. We utilize the tools from stochastic geometry to investigate two scenarios in which the TN downlink (DL) transmission is subject to interference from either satellites or NTN UEs transmitting in uplink (UL). Using the tools from stochastic geometry facilitates derivations of analytical exact expressions for the performance of the integrated TN-NTN network. The results herein provide direct insights on several parameters associated with the integrated network such as the satellite altitude, the TN user location, transmission power of BSs and satellites, traffic load, and ISD.

## B. Contributions and Paper Organization

In this paper, we consider a group of TN BSs distributed over a finite region which is also under the coverage of a beam from a LEO satellite. The TN and LEO networks share the same frequency channels in S-band. The UEs, located further away from the TN network's coverage area, lack access to the service provided by the TN network and, thus, are served by the LEO network. In order to analyze the performance of the integrated network and utilize the tools from stochastic geometry, we model the TN BSs and the NTN UEs as a BPP. The choice of BPP is justifiable as i) BSs and/or NTN users are distributed over a finite region, and ii) the performance is location dependent [42].

The main scientific contributions of this paper are as follows:

- Using the tools from stochastic geometry, we derive exact analytical expressions for the probability of coverage and

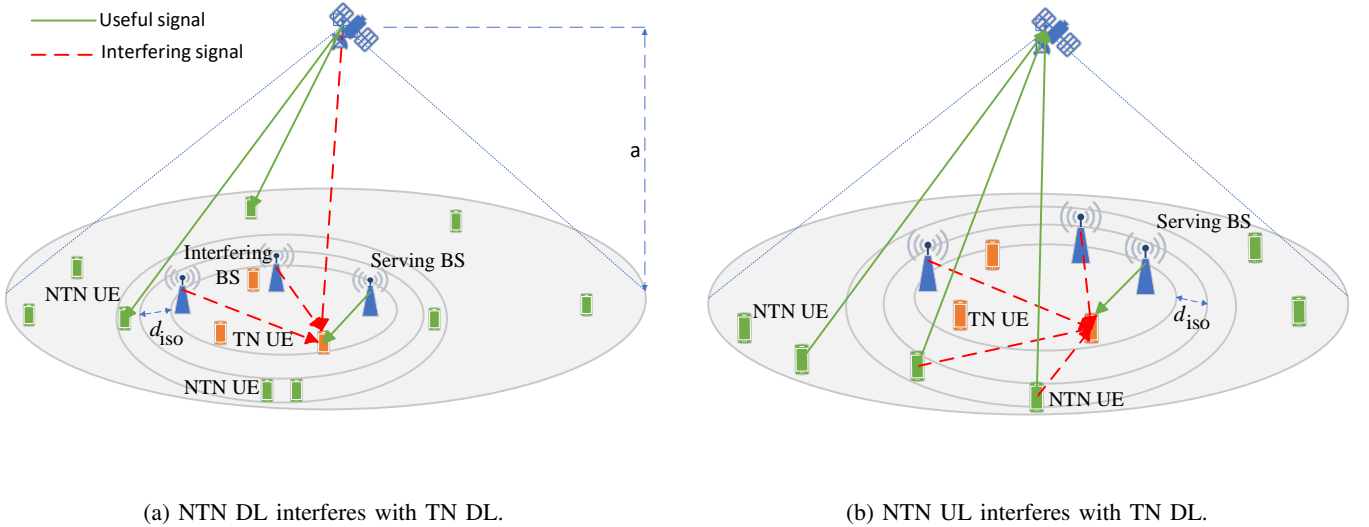


Fig. 1: Co-existence scenarios from [43] where NTN DL (a) or NTN UL (b) interferes with TN DL.

average achievable data rate of a TN DL network which shares the same frequency channel with NTN network.

- The performance analysis is provided for two co-existence cases which will be referred to as Case I and Case II in what follows. Case I corresponds to the case when TN network shares the same frequency channel with NTN in DL direction, i.e., the source of inter-network interference is from the satellite broadcasting the signal to the area where TN network is located. In Case II, the TN network shares the same frequency band with NTN in UL direction, i.e., the inter-network source of interference is from the NTN UEs transmitting to their serving satellite in close proximity of the TN network. Note that according to [44], the performance degradation in case of co-existence of TN UL with NTN network is insignificant.
- We validate all our theoretical derivations with Monte Carlo simulations. Throughout the numerical results, we show how each of the co-existence cases mentioned in the previous bullet point may affect the performance of TN network. The performance is illustrated in terms of several parameters, e.g., TN user's location in the cell, type of geographical environments, satellite's altitude, TN BS's transmit power, the number of NTN users, TN traffic load, and the isolation distance between TN and NTN UEs.
- The numerical results suggest several insightful guidelines on spectrum sharing between TN and NTN networks. In other words, the results provide the answer to the following question: *Given the network deployment parameters, user's distributions, and traffic load, which case of co-existence leads to a superior performance for the TN network?*

For the propagation model, we consider Nakagami- $m$  fading with integer  $m$  which not only preserves the analytical tractability but also covers a wide range of fading cases by varying the parameter  $m$ . As increasing  $m$  corresponds to

higher probability of line-of-sight, we opt a higher  $m$  for satellite to ground channels while a smaller value is used for terrestrial channels. From the numerical results, we will see that there is less performance degradation in urban regions when TN DL shares the same band with NTN DL. In the other scenario when NTN UL uses the same band as TN DL, the performance varies significantly with the TN user's location w.r.t. the cell center, i.e., more degradation occurs for edge users.

The remainder of this paper is organized as follows. Section II describes the system model as well as the two TN-NTN co-existence scenarios studied in this paper. Then in Section III, we derive the exact analytical expressions for the coverage performance and average data rate for each co-existence case. The verification of the analytical results as well as studying the effect of several network parameters on the performance of the integrated network is provided in Section IV. Finally, the paper is concluded in Section V.

## II. SYSTEM MODEL

The TN-NTN co-existence cases studied in this paper are shown in Fig. 1. In these cases, a LEO satellite orbiting at altitude  $a$  serves  $N_u$  NTN users in DL (c.f. Fig. 1(a)) and UL (c.f. Fig. 1(b)). Assuming that the TN network is always preferable over NTN due to its superior performance and reliability, NTN UEs are assumed to be distant from the TN network's edge at least by a distance denoted by  $d_{iso}$ . The TN BSs are distributed as clusters with radius  $r_{TN}$ , within the beam coverage area of the satellite, with each cluster having  $N_c$  BSs and the minimum distance between any two BSs, known as inter-site distance, is denoted by  $d_{ISD}$ , which is a function of the physical environment, e.g., rural, urban, etc. TN UEs are uniformly distributed within each TN cluster.

In this paper, the serving TN BS is assumed to be the nearest BS to the TN user and serves the TN UE in the DL direction. We assume that the same frequency band is shared among all TN BSs and with the NTN that provides coverage over

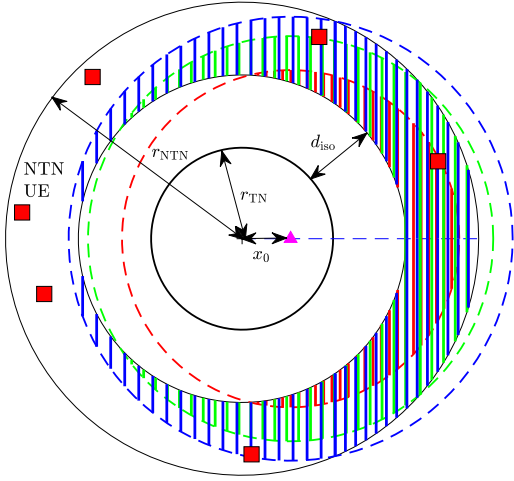


Fig. 2: Geometry of the system model used for derivation of (6) in co-existence Case II. The shaded area is the area obtained from the intersection of the disc centered at TN UE with radius  $R_n$  and the outer annulus defining the outer border for NTN UEs.

the TN cluster. This causes co-channel interference at the TN UE's reception. In Fig.1, solid lines represent the useful signals while dashed lines depict the interfering signals.

The channel model for serving link follows a Nakagami- $m$  fading model which allows to account for a wide range of multi-path fading conditions by varying the parameter  $m$ , while preserving the analytical tractability. Following the same approach as in [34], [38], we do not need to limit the fading distribution of the interfering channels to any specific one for the analytical derivations, since it has no effect on the tractability of our analysis. Obviously, resorting to some specific channel models is required to generate the numerical results. As the  $m$  parameter represents the ratio between the received power of line-of-sight and non-line-of-sight components, a larger value should be opted for satellite to ground channel compared to terrestrial links with less line-of-sight probability. The channel gains for TN and NTN links are denoted by  $H_{\text{TN}}$  and  $H_{\text{NTN}}$ , respectively.

The antennas at the satellites and TN BSs are directional and the beamforming patterns are chosen according to specifications given in [43]. The antennas can radiate multiple beams towards the ground. The TN and NTN users are equipped with omni-directional antenna elements. Assuming perfect beamforming, the overall maximum antenna gain will be expressed as  $G_{\text{NTN}} = G_{\text{sat}}G_{\text{u}}$  and  $G_{\text{TN}} = G_{\text{BS}}G_{\text{u}}$ , where  $G_{\text{sat}}$ ,  $G_{\text{BS}}$ , and  $G_{\text{u}}$  are the maximum antenna gain of satellites, the TN BSs, and the user, respectively.

We study the TN-NTN co-existence under two different scenarios as described in the following subsections. In these scenarios, we study the performance degradation caused by spectrum sharing between TN and NTN networks at the TN UE during NTN network transmission in DL and UL. Based on the described scenarios, the signal-to-interference-

plus-noise ratio (SINR) at the TN UE can be expressed as

$$\text{SINR} = \frac{p_{\text{TN}}G_{\text{TN}}H_{\text{TN}}R_0^{-\alpha_{\text{TN}}}}{I_{\text{TN}} + I_{\text{NTN}} + \sigma^2}, \quad (1)$$

where constant  $\sigma^2$  is the power of additive thermal noise, the parameter  $\alpha_{\text{TN}}$  is a path loss exponent for TN link,  $p_{\text{TN}}$  is the transmit power of TN BS,  $I_{\text{TN}} = \sum_{n=1}^{N_c-1} p_{\text{TN}}G_{\text{TN}}H_{\text{TN}}R_n^{-\alpha_{\text{TN}}}$  is the cumulative interference power from all other BSs in the same cluster as the TN user, and  $I_{\text{NTN}} \in \{I_{\text{DL}}, I_{\text{UL}}\}$  is the interference power received from the NTN network in DL and UL directions denoted by  $I_{\text{DL}}$  and  $I_{\text{UL}}$ , respectively. The distances from the TN user to the serving TN BS and other interfering BSs are denoted by random variables  $R_0$  and  $R_n$ ,  $n = 1, 2, \dots, N_c - 1$ , respectively. In the following subsections, we elaborate on two TN-NTN co-existence cases studied in this paper.

#### A. Co-existence Case I: NTN DL as the aggressor and TN DL as the victim

Co-existence Case I corresponds to Scenario 3 given in [43], in which both TN and NTN operate in DL over the same frequency band (c.f. Fig.1a). The aggressor in this case is a LEO satellite at altitude  $a$  and the victim is a TN user, which receives the useful signal from a BS. The source of interference at the TN UE will be from other BSs located in the same cluster with the TN UE and the serving BS, as well as the LEO satellite that provides coverage over the TN cluster.

We assume that BSs are distributed according to a BPP on a circle with radius  $r_{\text{TN}}$ , and that the victim TN UE, without loss of generality, is located on point  $(x_0, 0, 0)$ . Now let us define a circle centered at UE's location with radius equal to the distance between the UE and any BS in the TN cluster, denoted by  $R_n$ . The area of this circle is given by

$$\mathcal{A}(r_n) = \begin{cases} \pi r_n^2, & 0 \leq r_n \leq r_{\text{TN}} - x_0 \\ r_n^2 \left( \theta - \frac{1}{2} \sin(2\theta) \right) \\ + r_{\text{TN}}^2 \left( \phi - \frac{1}{2} \sin(2\phi) \right), & r_{\text{TN}} - x_0 < r_n < r_{\text{TN}} + x_0, \\ 0, & \text{otherwise.} \end{cases} \quad (2)$$

where  $\theta = \arccos\left(\frac{r_n^2 + x_0^2 - r_{\text{TN}}^2}{2x_0r_n}\right)$  and  $\phi = \arccos\left(\frac{-r_n^2 + x_0^2 + r_{\text{TN}}^2}{2x_0r_{\text{TN}}}\right)$ . Thus, for BPP-distributed BSs, the cumulative distribution function (CDF) of the distance between the TN UE and any arbitrary BS is  $F_{R_n}(r_n) = \frac{\mathcal{A}(r_n)}{\pi r_{\text{TN}}^2}$ . Due to the channel assignment by which the serving BS is the nearest one among all the  $N_c$  i.i.d. BSs, the CDF of  $R_0$  for a cluster of BPP distributed gNBs can be written as (3).

When conditioned on the serving distance such that  $R_0 = r_0$ , the CDF of  $R_n|R_0=r_0$  is obtained by conditioning  $R_n$  on  $R_0$  as follows:

$$\begin{aligned} F_{R_n|R_0}(r_n|r_0) &\triangleq \mathbb{P}(R_n < r_n | R_0 = r_0) \\ &= \frac{\mathbb{P}(r_0 \leq R_n \leq r_n)}{\mathbb{P}(R_n > r_0)} = \frac{F_{R_n}(r_n) - F_{R_n}(r_0)}{1 - F_{R_n}(r_0)}. \end{aligned} \quad (4)$$

$$\begin{aligned}
F_{R_0}(r_0) &\triangleq \mathbb{P}(R_0 \leq r_0) = 1 - (1 - F_R(r_0))^{N_c} \\
&= \begin{cases} 1 - \left(1 - \left(\frac{r_0}{r_{\text{TN}}}\right)^2\right)^{N_c}, & 0 \leq r_0 \leq r_{\text{TN}} - x_0 \\ 1 - \left(1 - \frac{1}{\pi} \left(\left(\frac{r_0}{r_{\text{TN}}}\right)^2 \left(\theta - \frac{1}{2} \sin(2\theta)\right) + \left(\phi - \frac{1}{2} \sin(2\phi)\right)\right)\right)^{N_c}, & r_{\text{TN}} - x_0 < r_0 \leq r_{\text{TN}} + x_0, \\ 0, & \text{otherwise.} \end{cases}
\end{aligned} \tag{3}$$

Taking the derivative w.r.t.  $r_n$  gives the probability density function (PDF) of  $R_n$  as

$$f_{R_n|R_0}(r_n|r_0) = \frac{f_{R_n}(r_n)}{1 - F_R(r_0)}. \tag{5}$$

The interference power received from a satellite transmitting towards the ground users, i.e.,  $I_{\text{NTN}}$  in (1), can be obtained as  $I_{\text{DL}} = p_{\text{NTN}} G_{\text{NTN}} H_{\text{NTN}} \mathcal{R}_n^{-\alpha_{\text{NTN}}}$ , where  $\mathcal{R}_n$  is the distance between the LEO satellite and the ground users, and  $\alpha_{\text{NTN}}$  is a path loss exponent for NTN link.

### B. Co-existence Case II: NTN UL as the aggressor and TN DL as the victim

Co-existence Case II corresponds to Scenario 5 given in [43] in which TN DL and NTN UL send the data over the same frequency band (c.f. Fig.1b). The aggressors in this case are the NTN UEs and the victim, similarly to Case I, is the TN UE, which receives the useful signal from its nearest TN BS. Thus, the source of interference at the TN UE will be from other NTN UEs, located at the edge of the TN UE cluster, and other BSs sharing the same cluster with the serving BS. Therefore, the serving distance distribution and TN interfering distances distribution will be similar to Case I as given in (3) and (4), respectively. The NTN interference power can be written as  $I_{\text{UL}} = \sum_{n=1}^{N_u} p_{\text{NTN}} G_{\text{NTN}} H_{\text{NTN}} \mathcal{R}_n^{-\alpha_{\text{TN}}}$ .

To obtain the distribution of the distances between the TN UE and NTN UEs, we assume that NTN UEs are distributed according to a BPP on the annulus between two concentric circles with radii  $r_{\text{TN}} + d_{\text{iso}}$  and  $r_{\text{NTN}}$  where  $r_{\text{TN}} + d_{\text{iso}} < r_{\text{NTN}}$  and  $d_{\text{iso}} \geq 0$ , as depicted in Fig. 2. Obviously, in this case, the interfering distances are independent of the serving distance. Thus, the distribution is not conditional on  $R_0$ . The distances from the TN UE to any NTN UE is denoted by  $\mathcal{R}_n$  to distinguish it from  $R_n$ , the distances between TN BSs and TN UE. The CDF of  $\mathcal{R}_n(\tau_n)$  is obtained as the ratio of the shaded region area shown in Fig 2 to the total surface area of the annulus where NTN UEs are distributed as a BPP. The shaded area is the area obtained from the intersection of the disc centered at TN UE with radius  $\mathcal{R}_n$  and the outer annulus.

The CDF  $F_{\mathcal{R}_n}(\tau_n) = \frac{\mathcal{A}(\tau_n)}{\pi(r_{\text{NTN}}^2 - (r_{\text{TN}} + d_{\text{iso}})^2)}$  is a piece-wise function given in (6), where  $\mathcal{A}(\tau_n)$  is the area of shaded region,  $w = r_{\text{TN}} + d_{\text{iso}}$ ,  $F_{a,b}(y) = (y - b)\sqrt{a^2 - (b - y)^2} + a^2 \tan^{-1}\left(\frac{y - b}{\sqrt{a^2 - (b - y)^2}}\right)$ . As can be seen from (6), the distribution of interfering distances depends on the location of TN user and the geometry of the network in terms of  $r_{\text{TN}}$ ,  $d_{\text{iso}}$ , and  $r_{\text{NTN}}$ . The PDF of  $\mathcal{R}_n$  can be obtained by taking the derivative w.r.t.  $\tau_n$ .

### III. EXACT PERFORMANCE ANALYSIS

In this section, we focus on the performance analysis of the integrated network for the scenarios described in Section II, in terms of coverage probability and data rate of a TN UE which is arbitrarily located on Earth. We utilize stochastic geometry in order to formulate coverage probability and rate as a function of the network's parameters and the propagation characteristics of the channels. One main component of our analytical derivations is the Laplace function of interference which will be presented throughout this section for both cases.

#### A. Performance Analysis for Coexistence Case I: NTN DL as the aggressor and TN DL as the victim

We define the coverage probability as the probability that the SINR at the TN UE's receiver is greater than a minimum required SINR, denoted by  $T$ . Thus, we have

$$P_c(T) \triangleq \mathbb{P}(\text{SINR} > T). \tag{7}$$

Based on the above given definition, in the following theorem, we derive an analytical expression for the probability of coverage for co-existence case I over a Nakagami- $m$  fading serving channel.

**Theorem 1.** *The coverage probability for a TN user in Co-existence Case I is*

$$\begin{aligned}
P_c(T) &= \int_0^{r_{\text{TN}} + x_0} f_{R_0}(r_0) \left[ e^{-s\sigma^2} \right. \\
&\quad \left. \sum_{k=0}^{m-1} \frac{\sum_{l=0}^k \binom{k}{l} (s\sigma^2)^l (-s)^{k-l} \frac{\partial^{k-l}}{\partial s^{k-l}} (\mathcal{L}_{I_{\text{TN}}}(s) \mathcal{L}_{I_{\text{DL}}}(s))}{k!} \right]_{s=s_c} dr_0,
\end{aligned} \tag{8}$$

where  $s_c = \frac{mT r_0^{\alpha_{\text{TN}}}}{p_{\text{TN}} G_{\text{TN}}}$ ,  $\mathcal{L}_{I_{\text{TN}}}(s)$  and  $\mathcal{L}_{I_{\text{DL}}}(s)$  are the Laplace transform of cumulative interference power  $I_{\text{TN}}$  and  $I_{\text{DL}}$  which are expressed in Lemma 1 and Lemma 2, respectively.

*Proof.* See Appendix A.  $\square$

**Lemma 1.** *Laplace function of cumulative interference power  $I_{\text{TN}}$  under general fading channels is*

$$\begin{aligned}
\mathcal{L}_{I_{\text{TN}}}(s) &\triangleq \mathbb{E}_{I_{\text{TN}}} [e^{-sI_{\text{TN}}}] \\
&= \left( \int_{r_0}^{r_{\text{TN}} + x_0} \mathcal{L}_{H_{\text{TN}}}(s p_{\text{TN}} G_{\text{TN}} r_n^{-\alpha_{\text{TN}}}) f_{R_n|R_0}(r_n|r_0) dr_n \right)^{N_c}.
\end{aligned} \tag{9}$$

*Proof.* See Appendix B  $\square$

$$\begin{aligned}
F_{\mathcal{R}_n}(\zeta_n) &= \frac{1}{\pi(r_{\text{NTN}}^2 - (r_{\text{TN}} + d_{\text{iso}})^2)} \times & (6) \\
\left\{ \begin{array}{ll}
0, & 0 \leq \mathcal{R}_n \leq w - x_0, \\
F_{w,0} \left( \frac{w^2 - \zeta_n^2 + x_0^2}{2x_0} \right) - F_{\zeta_n, x_0} \left( \frac{w^2 - \zeta_n^2 + x_0^2}{2x_0} \right) + F_{\zeta_n, x_0}(x_0 + \zeta_n) - F_{w,0}(w), & w - x_0 < \zeta_n \leq r_{\text{NTN}} - x_0, \\
F_{w,0} \left( \frac{w^2 - \zeta_n^2 + x_0^2}{2x_0} \right) - F_{\zeta_n, x_0} \left( \frac{w^2 - \zeta_n^2 + x_0^2}{2x_0} \right) + F_{\zeta_n, x_0} \left( \frac{r_{\text{NTN}}^2 - \zeta_n^2 + x_0^2}{2x_0} \right) + & r_{\text{NTN}} - x_0 < \zeta_n \leq w + x_0, \\
F_{r_{\text{NTN}},0}(r_{\text{NTN}}) - F_{w,0}(w) - F_{r_{\text{NTN}},0} \left( \frac{r_{\text{NTN}}^2 - \zeta_n^2 + x_0^2}{2x_0} \right), & \\
\pi(\zeta_n^2 - w^2) - F_{r_{\text{NTN}},0}(r_{\text{NTN}}) - F_{\zeta_n, x_0}(x_0 + \zeta_n) + & w + x_0 \leq \zeta_n \leq r_{\text{NTN}} + x_0, \\
F_{\zeta_n, x_0} \left( \frac{r_{\text{NTN}}^2 - \zeta_n^2 + x_0^2}{2x_0} \right) + F_{r_{\text{NTN}},0} \left( \frac{r_{\text{NTN}}^2 - \zeta_n^2 + x_0^2}{2x_0} \right), & \\
1, & \text{otherwise.}
\end{array} \right.
\end{aligned}$$

**Lemma 2.** Laplace function of cumulative interference power  $I_{\text{TN}}$  under general fading channels is

$$\begin{aligned}
\mathcal{L}_{I_{\text{DL}}}(s) &\triangleq \mathbb{E}_{\mathcal{R}_n, I_{\text{DL}}} [e^{-sI_{\text{DL}}}] = \\
&\int_a^{r_{\text{max}}} \mathbb{E}_{H_{\text{NTN}}} [\exp(-sp_{\text{NTN}}G_{\text{NTN}}H_{\text{NTN}}\zeta_n^{-\alpha_{\text{NTN}}})] f_{\mathcal{R}_n}(\zeta_n) d\zeta_n \\
&= \int_a^{r_{\text{max}}} \mathcal{L}_{H_{\text{NTN}}}(sp_{\text{NTN}}G_{\text{NTN}}\zeta_n^{-\alpha_{\text{NTN}}}) f_{\mathcal{R}_n}(\zeta_n) d\zeta_n, \quad (10)
\end{aligned}$$

where  $f_{\mathcal{R}_n}(\zeta_n)$  is the PDF of the distance between the satellite and a TN user which can be obtained from [34, Lemma 1], and  $r_{\text{max}} = \sqrt{2r_{\oplus}a + a^2}$  denotes the maximum possible distance between a satellite and a UE that is realized when the satellite is at the user's horizon.

*Proof.* The Laplace function is obtained by taking expectations over the two random variables, i.e., the distance between the LEO satellite and TN UE,  $\mathcal{R}_n$ , and the channel gain  $H_{\text{NTN}}$ .  $\square$

As a result, assuming some specific fading distributions,  $\mathcal{L}_{H_{\text{NTN}}}(\cdot)$  can be specified at the point  $sp_{\text{NTN}}G_{\text{NTN}}\zeta_n^{-\alpha_{\text{NTN}}}$ . In other words, the Laplace transform of NTN interference for any fading distribution can be calculated using Lemma 2. For instance, when  $H_{\text{NTN}}$  has a gamma distribution<sup>1</sup>,  $\mathcal{L}_{H_{\text{NTN}}}(sp_{\text{NTN}}G_{\text{NTN}}\zeta_n^{-\alpha_{\text{NTN}}}) = \frac{m^m}{(m + sp_{\text{NTN}}G_{\text{NTN}}\zeta_n^{-\alpha_{\text{NTN}}})^m}$ , where  $m$  is the Nakagami- $m$  fading parameter. Assuming LEO satellite to be at the zenith of the user, the Laplace function in Lemma 2 will be further simplified to  $\mathcal{L}_{I_{\text{DL}}}(s) = \frac{m^m}{(m + sp_{\text{NTN}}G_{\text{NTN}}a^{-\alpha_{\text{NTN}}})^m}$ .

The average achievable data rate (in bit/s/Hz) is defined as the ergodic capacity for a fading communication link which is derived from Shannon-Hartley theorem and normalized to unit bandwidth. The average achievable rate is defined as

$$\bar{C} \triangleq \mathbb{E}[\log_2(1 + \text{SINR})]. \quad (11)$$

In the following theorem, we derive the expression for the average rate of the victim TN user over Nakagami- $m$  fading serving channel. Both TN and NTN interfering channels may follow any arbitrary distribution.

<sup>1</sup>The gain of the channel, which is the square of Nakagami random variable, follows a gamma distribution.

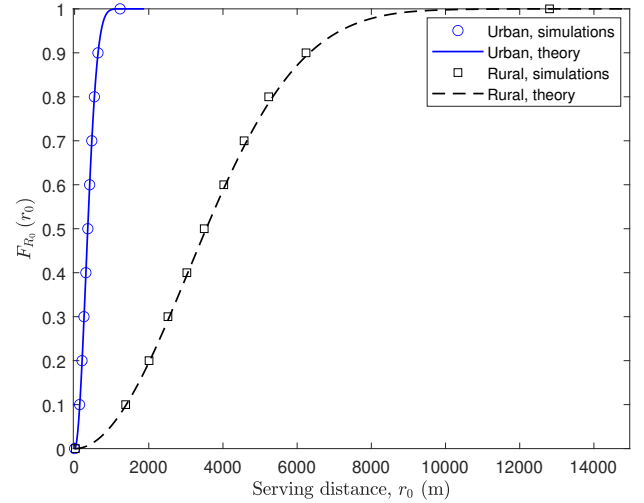


Fig. 3: Verification of serving distance distribution given in (3) for urban (ISD = 0.75 km) and rural (ISD = 7.5 km) areas.

**Theorem 2.** The average achievable rate for a TN user in Co-existence Case I is

$$\begin{aligned}
\bar{C} &= \int_0^{r_{\text{TN}} + x_0} \int_0^{\infty} f_{R_0}(r_0) \left[ e^{-s\sigma^2} \right. \\
&\left. \sum_{k=0}^{m-1} \sum_{l=0}^k \binom{k}{l} (s\sigma^2)^l (-s)^{k-l} \frac{\partial^{k-l}}{\partial s^{k-l}} (\mathcal{L}_{I_{\text{TN}}}(s)\mathcal{L}_{I_{\text{DL}}}(s)) \right]_{s=s_r} dt dr_0, \quad (12)
\end{aligned}$$

where  $s_r = \frac{m(2^t - 1)r_0^{\alpha_{\text{TN}}}}{p_{\text{TN}}G_{\text{TN}}}$ ,  $\mathcal{L}_{I_{\text{TN}}}(s)$  and  $\mathcal{L}_{I_{\text{DL}}}$  are obtained from Lemmas 1 and 2, respectively.

*Proof.* See Appendix C.  $\square$

**B. Performance Analysis for Co-existence Case II: NTN UL as the aggressor and TN DL as the victim**

In the following theorem, we analytically formulate the probability of coverage for co-existence case II, utilizing the definition provided earlier in (7). Similar to Theorem 1, the

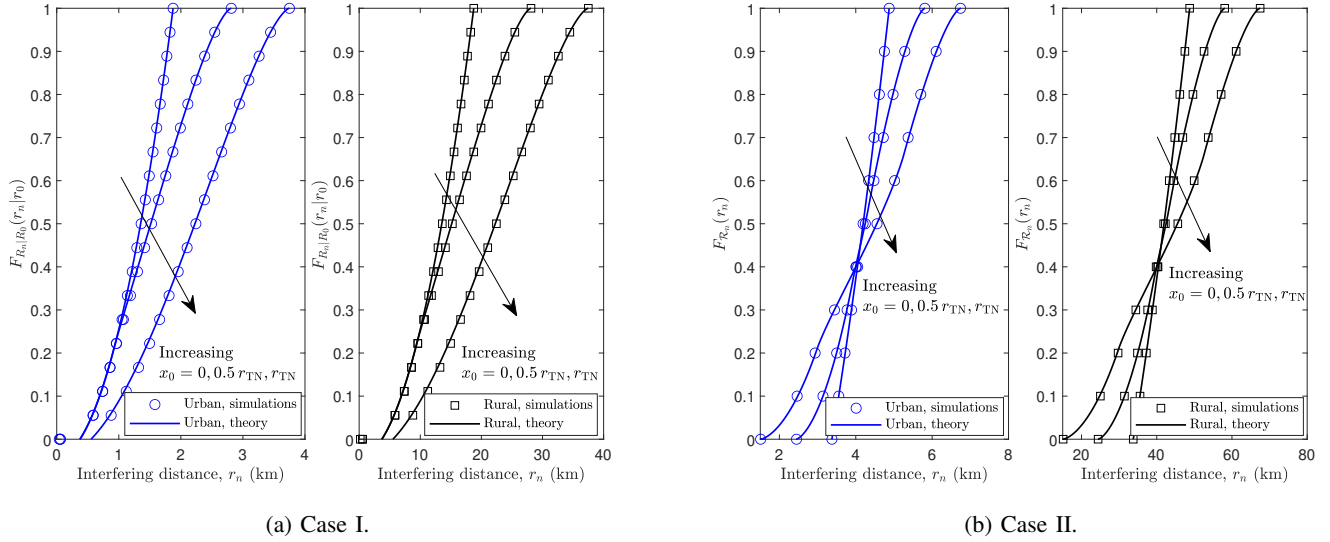


Fig. 4: Verification of the interfering distance distribution, for cases I (a), given as in (4), and II (b) given as in (4).

serving channel follows a Nakagami- $m$  distribution while interfering channels may follow arbitrary distributions.

**Theorem 3.** *The coverage probability for a TN user in Co-existence Case II is*

$$P_c(T) = \int_0^{r_{\text{TN}}+x_0} f_{R_0}(r_0) \left[ e^{-s\sigma^2} \sum_{k=0}^{m-1} \frac{\sum_{l=0}^k \binom{k}{l} (s\sigma^2)^l (-s)^{k-l} \frac{\partial^{k-l}}{\partial s^{k-l}} (\mathcal{L}_{I_{\text{TN}}}(s) \mathcal{L}_{I_{\text{UL}}}(s))}{k!} \right]_{s=s_c} dr_0, \quad (13)$$

where  $s_c = \frac{mT r_0^{\alpha_{\text{TN}}}}{p_{\text{TN}} G_{\text{TN}}}$ , and  $\mathcal{L}_{I_{\text{UL}}}(s)$  is the Laplace transform of cumulative interference power  $I_{\text{UL}}$  from all NTN UEs located on the outer annulus shown in Fig. 2 that is expressed in Lemma 3. Obviously,  $\mathcal{L}_{I_{\text{TN}}}(s)$  remains the same as for Case I and is obtained from Lemma 1.

*Proof.* The expression can be obtained using similar steps as shown in the proof of Theorem 1 given in Appendix A by only substituting  $I_{\text{UL}} \rightarrow I_{\text{DL}}$ .  $\square$

**Lemma 3.** *Laplace function of cumulative interference power  $I_{\text{UL}}$  under general fading channels is*

$$\mathcal{L}_{I_{\text{UL}}}(s) \triangleq \mathbb{E}_{I_{\text{UL}}} [e^{-sI_{\text{UL}}}] \quad (14)$$

$$= \left( \int_{w-x_0}^{r_{\text{NTN}}+x_0} \mathcal{L}_{H_{\text{NTN}}}(s p_{\text{NTN}} G_{\text{NTN}} \tau_n^{-\alpha_{\text{TN}}}) f_{R_n}(\tau_n) d\tau_n \right)^{N_u}$$

*Proof.* See Appendix D  $\square$

In the following theorem, we formulate the expression for the average rate of the victim TN user over Nakagami- $m$  fading serving channel for co-existence Case II.

**Theorem 4.** *The average achievable rate for a TN user in Co-existence Case II is*

$$\bar{C} = \int_0^{r_{\text{TN}}+x_0} \int_0^\infty f_{R_0}(r_0) \left[ e^{-s\sigma^2} \sum_{k=0}^{m-1} \frac{\sum_{l=0}^k \binom{k}{l} (s\sigma^2)^l (-s)^{k-l} \frac{\partial^{k-l}}{\partial s^{k-l}} (\mathcal{L}_{I_{\text{TN}}}(s) \mathcal{L}_{I_{\text{UL}}}(s))}{k!} \right]_{s=s_r} dt dr_0, \quad (15)$$

where  $s_r = \frac{m(2^t-1)r_0^{\alpha_{\text{TN}}}}{p_{\text{TN}} G_{\text{TN}}}$ .  $\mathcal{L}_{I_{\text{TN}}}(s)$  and  $\mathcal{L}_{I_{\text{UL}}}(s)$  are obtained from Lemmas 1 and 3, respectively.

*Proof.* The proof follows similar procedure as shown in the proof of Theorem 2 presented in Appendix C. The sole difference is the origin of NTN cumulative interference power, which, in this case, arises from NTN UL.  $\square$

#### IV. NUMERICAL RESULTS

In this section, the analytical derivations on the performance of the integrated network for each case is verified through Monte Carlo simulations. The TN BSs, satellites, and UEs antenna models are chosen according to the sectorized antenna patterns given in [43] for simulations. However, in order to maintain tractability for the theoretical results, we approximate such model by assuming fixed antenna gains for the main and side lobes of the antennas, similar to [45]–[47]. In fact, the main beam transmits with the maximum antenna gain given in [43], while side lobes are assumed to have 13 dB lower gain, similar to [45], [48].

We consider the path-loss exponents to be  $\alpha_{\text{TN}} = 3$  and  $\alpha_{\text{NTN}} = 2$  for TN and NTN propagation channels, respectively, according to [49, Table 3.2]. We adopt a practical fading model, i.e., Rician, for all simulation results with parameter  $K$ , where  $K = 0$  and 200 for TN and NTN channels, respectively, to account for higher LoS in NTN. Since the theoretical derivations are developed assuming a Nakagami- $m$  fading for the

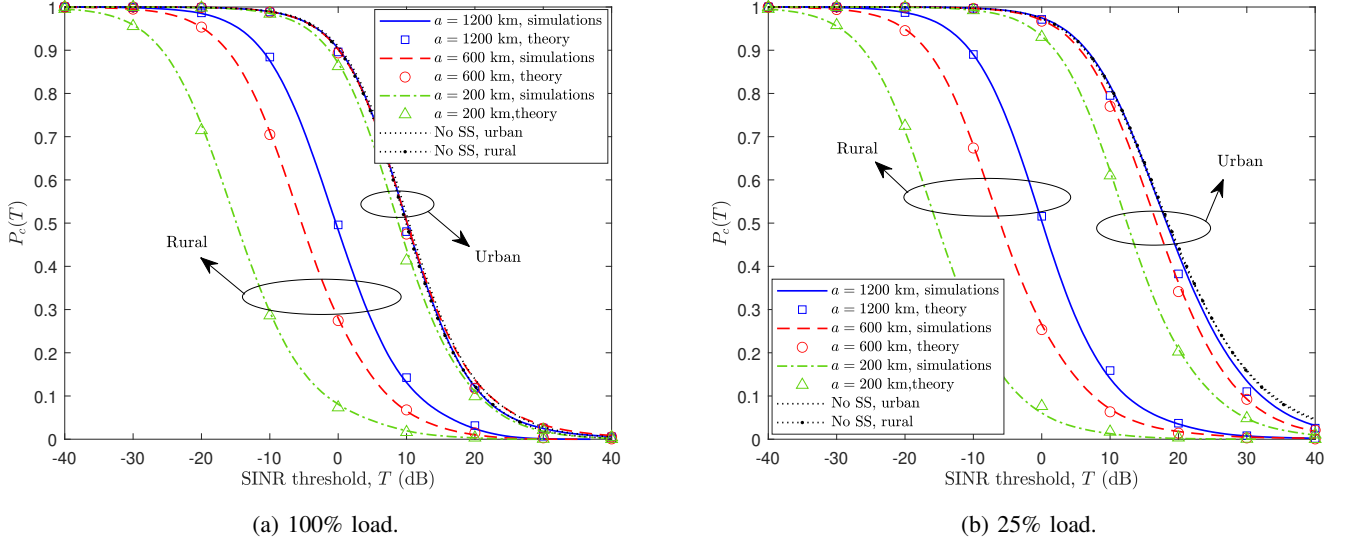


Fig. 5: Coverage probability of Case I for 100% load (a), and 25% load (b), for different LEO satellite altitudes. The simulations, shown by lines, verify the theoretical results, depicted by markers, given in Theorem 1.

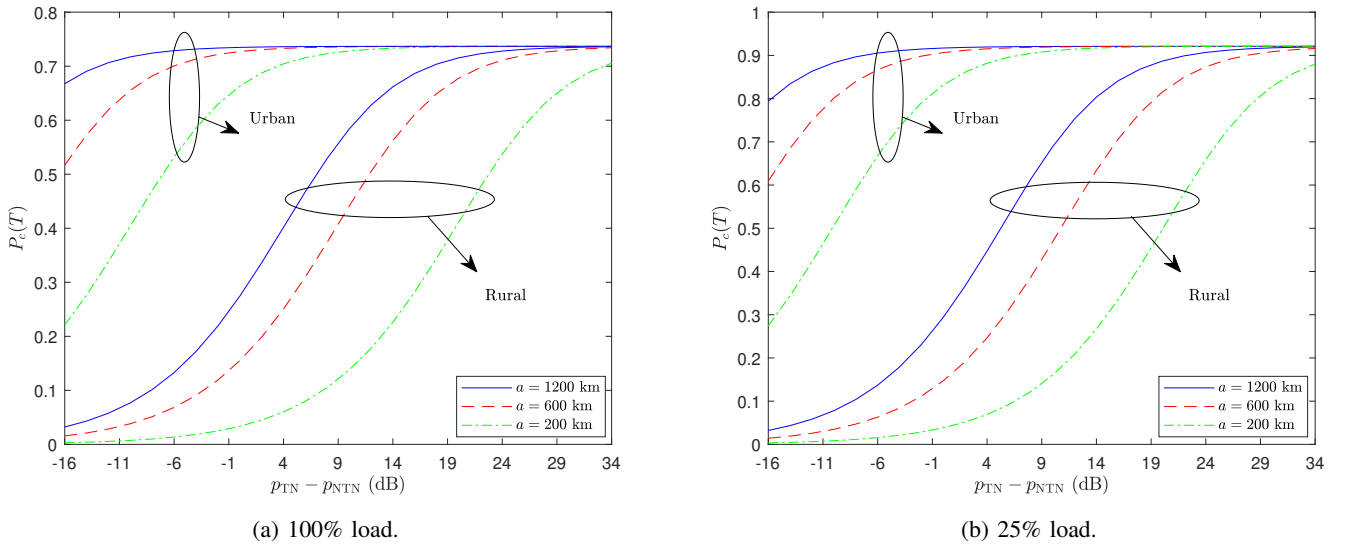


Fig. 6: Effect of transmit power on coverage probability of Case I for 100% load (a), and 25% load (b).

serving link to preserve the analytical tractability, a Nakagami- $m$  distribution is used for their numerical calculations by setting its parameter to  $m = \frac{k^2 + 2K + 1}{2K + 1}$ , by matching the first and second moments of Rician and Nakagami PDFs. The fair match between theoretical results and simulations confirms the high accuracy of such approximation.

The satellite transmit power, cell radius, maximum antenna gain are  $p_t = 46$  dBm, 25 km, and 30 dBi, respectively. The main lobe gain of the BSs antennas is assumed to be 17 dBi. The BS transmit power is assumed to be  $p_t = 46$  dBm. The altitude is set to  $\{200, 600, 1200\}$  km, unless stated otherwise. Inter-site distances for TN network are assumed to be 0.75 km and 7.5 km for urban and rural areas, respectively. The number of BSs on each TN cluster is assumed to be 19. The operating frequency and bandwidth are set to be 2 GHz and 20 MHz,

respectively.

Figure 3 verifies the derivation of serving distance distribution given in (3) for urban and rural areas. It is worth noting that the serving distance is the same for both Cases I and II. Figures 4(a) and 4(b) verify the CDF of interference from TN BSs and NTN UEs derived in (4) and (6), respectively, in rural and urban areas. The results are presented for a TN user located at the center, middle, and the edge of the TN cluster, i.e.,  $x_0 = \{0, 0.5 r_{TN}, r_{TN}\}$ . As can be seen in the figures 3 and 4, there is a perfect match between the analytical results, shown by lines, and the simulations, shown by markers, which verifies the exactness of the derivations.

Figures 5(a) and 5(b) verify the derivations in Theorem 1 for 100% and 25% load from the TN network. The load level represents what percentage of BSs are active within the TN



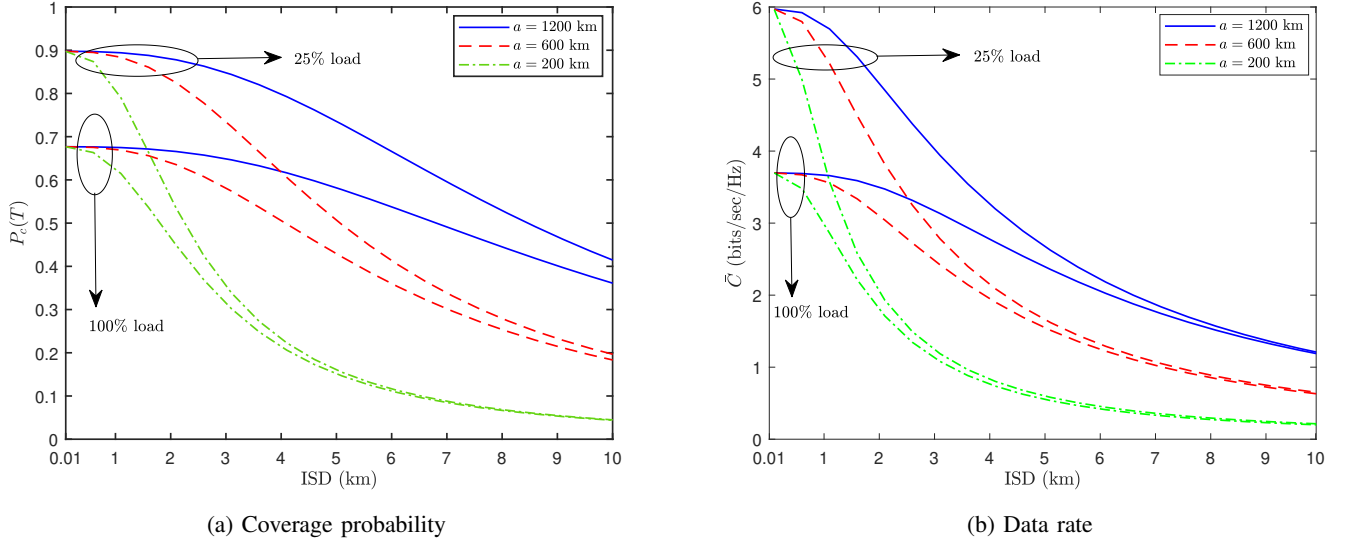


Fig. 7: Effect of ISD on Coverage probability (a) and data rate (b) of Case I for different LEO satellite altitudes and TN load levels.

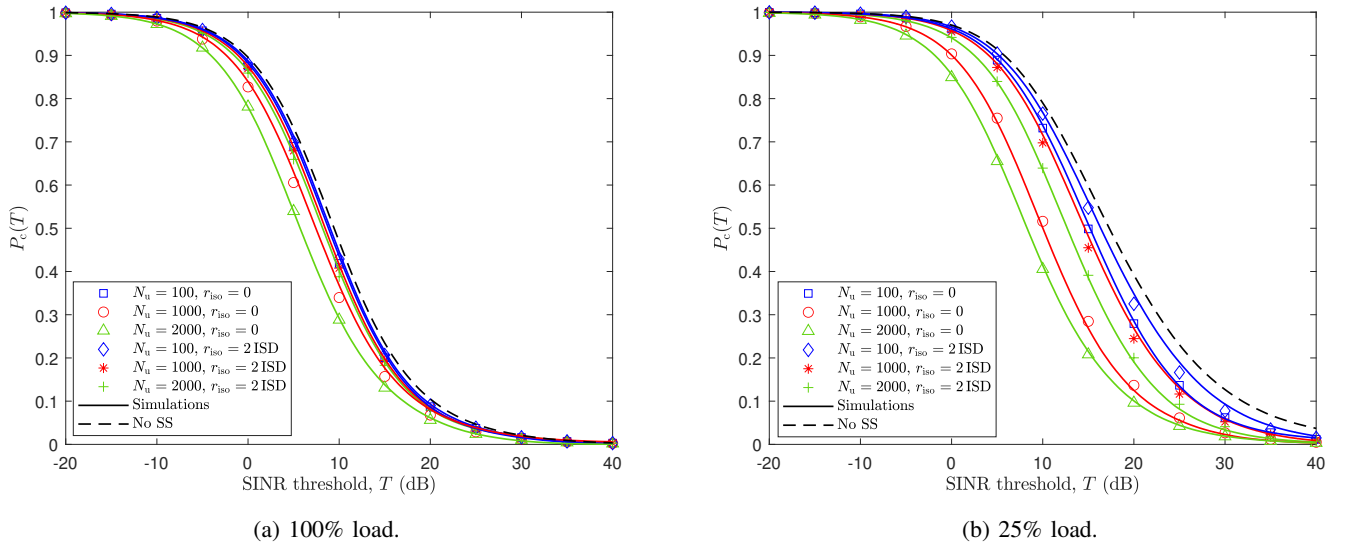


Fig. 8: Coverage probability of Case II for 100% load (a), and 25% load (b) for different number of NTN UEs and isolation distances. The simulations, shown by lines, verify the theoretical results, depicted by markers, given in Theorem 3.

cluster. The black dotted lines represent the case of having no spectrum sharing between TN and NTN, i.e., the whole band is allocated only to TN. We can observe that the performance degradation due to sharing the spectrum is less significant in urban areas. The reason is that BSs are located in relatively closer proximity, i.e., smaller ISD, in urban areas, such that the interference received from TN BSs is much larger than the interference received from the LEO satellite, especially for 100% load. On the other hand, for rural network, as the BSs are much farther from each other, NTN interference becomes more comparable to TN interference. Thus, there is more performance degradation for rural areas when sharing the spectrum between TN and NTN. Obviously, the impact of LEO satellite altitude is also more significant in rural regions.

Figures 6(a) and 6(b) show the effect of power allocation between TN and NTN on coverage probability. The transmit power of LEO satellite is assumed to be fixed and equal to  $p_{\text{NTN}} = 46$  dBm. By increasing the TN power, the coverage probability saturates to a fixed value for which the NTN has no effect on its performance. The saturation value depends on the number of interfering TN BSs. As can be seen from the figure, a higher TN power is required for larger ISD distances, i.e., rural regions, as well as for lower satellite altitudes to maximize the coverage probability.

The effect of ISD for different satellites altitudes and TN load levels on coverage probability and data rate are illustrated in Figs. 7(a) and 7(b), respectively. Lower ISD provides better coverage and rate due to more strength of the serving signal.

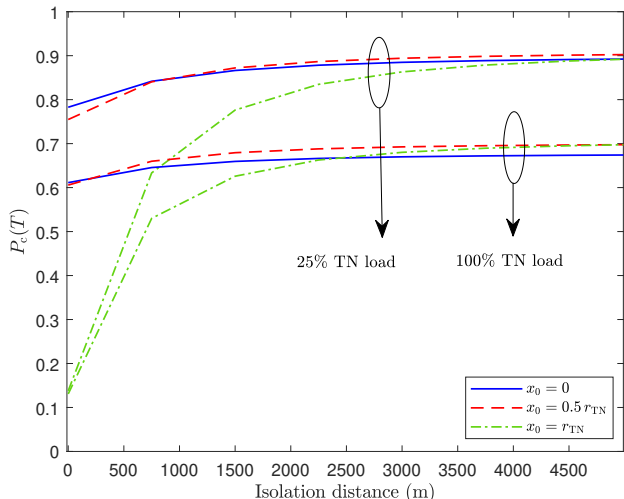


Fig. 9: Effect of isolation distance,  $d_{\text{iso}}$ , on coverage probability of Case II for different TN UE's locations.

The performance drops with increasing the ISD. The decrease is more considerable for lower LEO altitudes due to higher interference power.

For Case II, the transmit power of NTN UEs is assumed to be 200 mW with antenna gain of 1 dBi as specified in [43]. Figures 8(a) and 8(b) verify the derivations in Theorem 3 for 100% and 25% load from the TN cell and varying the number of NTN UEs and isolation distances. The results show that the interference from TN DL is more significant compared to NTN UL, especially for higher loads. The effect of spectrum sharing is rather minimal for 100% load from TN network, especially when isolation distance is greater than  $2d_{\text{ISD}}$ .

The effect of isolation distance between the TN and NTN networks is shown in Fig. 9, for  $a = 200$  km. As can be seen in the figure, increasing the isolation distance has no significant impact on the performance of users located at the center or middle of the TN cell. For edge users, a larger isolation distance is needed to achieve the highest possible performance. The minimum required isolation distance also decreases with increasing the TN load level since the NTN interference becomes less comparable to TN interference.

## V. CONCLUSIONS

In this paper, we studied the performance of integrated TN-NTN network when TN and NTN operate on the same frequency channel in S-band. Two co-existence cases were considered in which the TN users receive interference from either NTN DL or UL. Using tools from stochastic geometry, we obtained exact tractable expressions on the coverage probability and average data rate for each case in terms of TN and NTN networks' parameters. The analysis and results provided herein will pave the way for optimal dynamic spectrum sharing between TN and NTN. The study showed that, depending on the network parameters, one co-existence case may outperform the other in terms of the probability of coverage and average achievable rate. Thus, the network may dynamically switch

between the two cases to optimize the performance. It was also shown that there is a minimum isolation distance between TN and NTN which can minimize the effect of interference caused by spectrum sharing.

## APPENDIX

### A. Proof of Theorem 1

Let us start derivation of Theorem 1 using the definition of coverage probability given in (7):

$$\begin{aligned}
 P_c(T) &= \mathbb{P}(\text{SINR} > T) = \mathbb{E}_{R_0} [\mathbb{P}(\text{SINR} > T | R_0 = r_0)] \\
 &= \int_0^u \mathbb{P}(\text{SINR} > T | R_0 = r_0) f_{R_0}(r_0) dr_0 \\
 &= \int_0^u \mathbb{P}\left(\frac{p_{\text{TN}} G_{\text{TN}} H_{\text{TN}} r_0^{-\alpha_{\text{TN}}}}{I_{\text{TN}} + I_{\text{DL}} + \sigma^2} > T\right) f_{R_0}(r_0) dr_0 \\
 &= \int_0^u \mathbb{E}_{I_{\text{TN}}, I_{\text{DL}}} \left[ \mathbb{P}\left(H_{\text{TN}} > \frac{T(I_{\text{TN}} + I_{\text{DL}} + \sigma^2) r_0^{\alpha_{\text{TN}}}}{p_{\text{TN}} G_{\text{TN}}}\right) \Big| I_{\{\text{TN}, \text{DL}\}} > 0 \right] \\
 &\quad \times f_{R_0}(r_0) dr_0 \\
 &= \int_0^u \mathbb{E}_{I_{\text{TN}}, I_{\text{DL}}} \left[ 1 - F_{H_{\text{TN}}}\left(\frac{T(I_{\text{TN}} + I_{\text{DL}} + \sigma^2) r_0^{\alpha_{\text{TN}}}}{p_{\text{TN}} G_{\text{TN}}}\right) \right] \\
 &\quad \times f_{R_0}(r_0) dr_0 \\
 &\stackrel{(a)}{=} \int_0^u \mathbb{E}_{I_{\text{TN}}, I_{\text{DL}}} \left[ \frac{\Gamma\left(m, m \frac{T(I_{\text{TN}} + I_{\text{DL}} + \sigma^2) r_0^{\alpha_{\text{TN}}}}{p_{\text{TN}} G_{\text{TN}}}\right)}{\Gamma(m)} \right] f_{R_0}(r_0) dr_0 \\
 &\stackrel{(b)}{=} \int_0^u f_{R_0}(r_0) e^{-\frac{m T \sigma^2 r_0^{\alpha_{\text{TN}}}}{p_{\text{TN}} G_{\text{TN}}}} \mathbb{E}_{I_{\text{TN}}, I_{\text{DL}}} \left[ e^{-m \frac{T(I_{\text{TN}} + I_{\text{DL}}) r_0^{\alpha_{\text{TN}}}}{p_{\text{TN}} G_{\text{TN}}}} \right. \\
 &\quad \left. \sum_{k=0}^{m-1} \sum_{l=0}^k \binom{k}{l} \left(m \frac{T \sigma^2 r_0^{\alpha_{\text{TN}}}}{p_{\text{TN}} G_{\text{TN}}}\right)^l \left(m \frac{T(I_{\text{TN}} + I_{\text{DL}}) r_0^{\alpha_{\text{TN}}}}{p_{\text{TN}} G_{\text{TN}}}\right)^{k-l} \right] dr_0 \\
 &\stackrel{(c)}{=} \int_0^u f_{R_0}(r_0) \left[ e^{-s \sigma^2} \right. \\
 &\quad \left. \sum_{k=0}^{m-1} \sum_{l=0}^k \binom{k}{l} (s \sigma^2)^l (-s)^{k-l} \frac{\partial^{k-l}}{\partial s^{k-l}} \mathcal{L}_{I_{\text{TN}}}(s) \mathcal{L}_{I_{\text{DL}}}(s) \right]_{s=s_0} dr_0,
 \end{aligned} \tag{16}$$

where  $u = r_{\text{TN}} + x_0$ ,  $F_{H_{\text{TN}}}(\cdot)$  is the CDF of  $H_{\text{TN}}$ , (a) follows from the distribution of gamma random variable  $H_{\text{TN}}$  (being the square of the Nakagami random variable), (b) is calculated by applying the definition of incomplete gamma function for integer values of  $m$  to (a), and (c) follows from independence of  $I_{\text{TN}}$  and  $I_{\text{NTN}}$ , i.e.,  $\mathbb{E}_{I_{\text{TN}}, I_{\text{NTN}}} [e^{-s(I_{\text{TN}} + I_{\text{NTN}})}] = \mathbb{E}_{I_{\text{TN}}} [e^{-s I_{\text{TN}}}] \mathbb{E}_{I_{\text{NTN}}} [e^{-s I_{\text{NTN}}}]$ .

### B. Proof of Lemma 1

Using the definition of the Laplace transform yields

$$\begin{aligned}
\mathcal{L}_{I_{\text{TN}}}(s) &\triangleq \mathbb{E}_{I_{\text{TN}}} [e^{-sI_{\text{TN}}}] \\
&= \mathbb{E}_{R_n, H_{\text{TN}}} \left[ \exp \left( -s \sum_{n=1}^{N_c} p_{\text{TN}} G_{\text{TN}} H_{\text{TN}} R_n^{-\alpha_{\text{TN}}} \right) \right] \\
&= \mathbb{E}_{R_n, H_{\text{TN}}} \left[ \prod_{n=1}^{N_c} \exp \left( -s p_{\text{TN}} G_{\text{TN}} H_{\text{TN}} R_n^{-\alpha_{\text{TN}}} \right) \right] \\
&\stackrel{(a)}{=} \mathbb{E}_{R_n} \left[ \prod_{n=1}^{N_c} \mathbb{E}_{H_{\text{TN}}} \left[ \exp \left( -s p_{\text{TN}} G_{\text{TN}} H_{\text{TN}} R_n^{-\alpha_{\text{TN}}} \right) \right] \right] \\
&\stackrel{(b)}{=} \prod_{n=1}^{N_c} \int_{r_0}^u \mathbb{E}_{H_{\text{TN}}} \left[ \exp \left( -s p_{\text{TN}} G_{\text{TN}} H_{\text{TN}} r_n^{-\alpha_{\text{TN}}} \right) \right] \\
&\quad \times f_{R_n|R_0}(r_n|r_0) dr_n \\
&\stackrel{(c)}{=} \left( \int_{r_0}^u \mathcal{L}_{H_{\text{TN}}}(s p_{\text{TN}} G_{\text{TN}} r_n^{-\alpha_{\text{TN}}}) f_{R_n|R_0}(r_n|r_0) dr_n \right)^{N_c}, \tag{17}
\end{aligned}$$

where  $u = r_{\text{TN}} + x_0$ , (a) follows from the i.i.d. distribution of  $H_{\text{TN}}$  and its further independence from  $R_n$ , (b) is obtained using the interfering distance distribution from (5), and (c) is derived thanks to the i.i.d. distribution of conditional PDF of  $f_{R_n|R_0}(r_n|r_0)$  and the substitution from the definition of Laplace function.

### C. Proof of Theorem 2

Based on the definition of the average data rate given in (11), we have

$$\begin{aligned}
\bar{C} &= \mathbb{E}_{I_{\text{TN}}, I_{\text{DL}}, H_{\text{TN}}, R_0} [\log_2(1 + \text{SINR})] \\
&= \int_0^u \mathbb{E}_{I_{\text{TN}}, I_{\text{DL}}, H_{\text{TN}}} [\log_2(1 + \text{SINR})] f_{R_0}(r_0) dr_0 \tag{18} \\
&\stackrel{(a)}{=} \int_0^u \int_0^\infty \mathbb{E}_{I_{\text{TN}}, I_{\text{DL}}, H_{\text{TN}}} [\mathbb{P}(\log_2(1 + \text{SINR}) > t)] f_{R_0}(r_0) dt dr_0,
\end{aligned}$$

where  $u = r_{\text{TN}} + x_0$ ,  $\text{SINR} = \frac{p_{\text{TN}} G_{\text{TN}} H_{\text{TN}} r_0^{-\alpha_{\text{TN}}}}{I_{\text{TN}} + I_{\text{DL}} + \sigma^2}$ , and (a) is obtained from the fact that for a positive random variable  $X$ ,  $\mathbb{E}[X] = \int_{t>0} \mathbb{P}(X > t) dt$ . Thus, we have

$$\begin{aligned}
\bar{C} &\stackrel{(a)}{=} \tag{19} \\
&\int_0^u \int_0^\infty \mathbb{E}_{I_{\text{TN}}, I_{\text{DL}}} \left[ 1 - F_{H_{\text{TN}}} \left( \frac{r_0^{\alpha_{\text{TN}}} (I_{\text{TN}} + I_{\text{DL}} + \sigma^2) (2^t - 1)}{p_{\text{TN}} G_{\text{TN}}} \right) \right] \\
&\quad \times f_{R_0}(r_0) dt dr_0 \\
&\stackrel{(b)}{=} \int_0^u \int_0^\infty \mathbb{E}_{I_{\text{TN}}, I_{\text{DL}}} \left[ \frac{\Gamma \left( m, \frac{r_0^{\alpha_{\text{TN}}} (I_{\text{TN}} + I_{\text{DL}} + \sigma^2) (2^t - 1)}{p_{\text{TN}} G_{\text{TN}}} \right)}{\Gamma(m)} \right] \\
&\quad \times f_{R_0}(r_0) dt dr_0 \\
&\stackrel{(c)}{=} \int_0^u \int_0^\infty f_{R_0}(r_0) e^{-\frac{m \sigma^2 (2^t - 1) r_0^{\alpha_{\text{TN}}}}{p_{\text{TN}} G_{\text{TN}}}} \mathbb{E}_{I_{\text{TN}}, I_{\text{DL}}} \left[ e^{-m \frac{(I_{\text{DL}} + I_{\text{TN}}) r_0^{\alpha_{\text{TN}}}}{p_{\text{TN}} G_{\text{TN}}}} \right] \\
&\quad \sum_{k=0}^{m-1} \frac{\sum_{l=0}^k \binom{k}{l} \left( m \frac{\sigma^2 (2^t - 1) r_0^{\alpha_{\text{TN}}}}{p_{\text{TN}} G_{\text{TN}}} \right)^l \left( m \frac{(I_{\text{DL}} + I_{\text{TN}}) r_0^{\alpha_{\text{TN}}}}{p_{\text{TN}} G_{\text{TN}}} \right)^{k-l}}{k!} dt dr_0,
\end{aligned}$$

where (a) follows from the product distribution of two independent random variables, (b) follows from the gamma distribution of serving channel gain  $H_{\text{TN}}$ , and (c) is calculated by applying the incomplete gamma function for integer values of  $m$  to (b).

### D. Proof of Lemma 3

Using the definition of the Laplace transform yields

$$\begin{aligned}
\mathcal{L}_{I_{\text{UL}}}(s) &\triangleq \mathbb{E}_{I_{\text{UL}}} [e^{-sI_{\text{UL}}}] \\
&= \mathbb{E}_{\mathcal{R}_n, H_{\text{NTN}}} \left[ \exp \left( -s \sum_{n=1}^{N_u} p_{\text{NTN}} G_{\text{NTN}} H_{\text{NTN}} \mathcal{R}_n^{-\alpha_{\text{TN}}} \right) \right] \\
&= \mathbb{E}_{\mathcal{R}_n, H_{\text{NTN}}} \left[ \prod_{n=1}^{N_u} \exp \left( -s p_{\text{NTN}} G_{\text{NTN}} H_{\text{NTN}} \mathcal{R}_n^{-\alpha_{\text{TN}}} \right) \right] \\
&\stackrel{(a)}{=} \mathbb{E}_{\mathcal{R}_n} \left[ \prod_{n=1}^{N_u} \mathbb{E}_{H_{\text{NTN}}} \left[ \exp \left( -s p_{\text{NTN}} G_{\text{NTN}} H_{\text{NTN}} \mathcal{R}_n^{-\alpha_{\text{TN}}} \right) \right] \right] \\
&\stackrel{(b)}{=} \prod_{n=1}^{N_u} \int_{w-x_0}^{r_{\text{NTN}}+x_0} \mathbb{E}_{H_{\text{NTN}}} \left[ \exp \left( -s p_{\text{NTN}} G_{\text{NTN}} H_{\text{NTN}} \zeta_n^{-\alpha_{\text{TN}}} \right) \right] \\
&\quad \times f_{\mathcal{R}_n}(\zeta_n) d\zeta_n \\
&\stackrel{(c)}{=} \left( \int_{w-x_0}^{r_{\text{NTN}}+x_0} \mathcal{L}_{H_{\text{NTN}}}(s p_{\text{NTN}} G_{\text{NTN}} \zeta_n^{-\alpha_{\text{TN}}}) f_{\mathcal{R}_n}(\zeta_n) d\zeta_n \right)^{N_u}, \tag{20}
\end{aligned}$$

where  $w = r_{\text{TN}} + d_{\text{iso}}$ , (a) follows from the i.i.d. distribution of  $H_{\text{NTN}}$  and its further independence from  $\mathcal{R}_n$ , (b) is obtained using the derivative of interfering distance CDF from (6), (c) is derived thanks to the i.i.d. distribution of PDF of  $f_{\mathcal{R}_n}(\zeta_n)$  and the substitution from the definition of Laplace function.

### REFERENCES

- [1] H. Xie, Y. Zhan, G. Zeng, and X. Pan, "LEO mega-constellations for 6G global coverage: Challenges and opportunities," *IEEE Access*, vol. 9, pp. 164 223–164 244, 2021.
- [2] X. Lin, S. Cioni, G. Charbit, N. Chuberre, S. Hellsten, and J.-F. Boutillon, "On the path to 6G: Embracing the next wave of low earth orbit satellite access," *IEEE Communications Magazine*, vol. 59, no. 12, pp. 36–42, 2021.
- [3] M. M. Azari, S. Solanki, S. Chatzinotas, O. Kodheli, H. Sallouha, A. Colpaert, J. F. Mendoza Montoya, S. Pollin, A. Haqiqatnejad, A. Mostaani, E. Lagunas, and B. Ottersten, "Evolution of non-terrestrial networks from 5G to 6G: A survey," *IEEE Communications Surveys and Tutorials*, vol. 24, no. 4, pp. 2633–2672, 2022.
- [4] F. Baccelli and B. Błaszczyszyn, "Stochastic geometry and wireless networks," *Foundations and Trends in Networking*, vol. 1, 2009.
- [5] M. López, S. B. Damsgaard, I. Rodríguez, and P. Mogensen, "An empirical analysis of multi-connectivity between 5G terrestrial and LEO satellite networks," in *Proc. Globecom Workshops*, 2022.
- [6] E. Souza, A. Linhares, C. Queiroz, L. Valle, U. Dias, and A. Barreto, "An open source simulation tool for sharing and compatibility studies between 5G and other radio communication systems," in *Proc. International Microwave and Optoelectronics Conference (IMOC)*, 2017.
- [7] C. Queiroz, R. Vieira, A. Barreto, A. Zarrebini, E. Souza, and A. Linhares, "New spectrum bands for HAPS: Sharing with fixed-satellite systems," in *Proc. IEEE 89th Vehicular Technology Conference*, 2019.
- [8] R. Smith, C. Freeberg, T. Machacek, and V. Ramaswamy, "An O-RAN approach to spectrum sharing between commercial 5G and government satellite systems," in *Proc. IEEE Military Communications Conference (MILCOM)*, 2021.
- [9] H.-W. Lee, A. Medles, V. Jie, D. Lin, X. Zhu, I.-K. Fu, and H.-Y. Wei, "Reverse spectrum allocation for spectrum sharing between TN and NTN," in *Proc. IEEE Conference on Standards for Communications and Networking (CSCN)*, 2021.

- [10] H. Kokkinen, A. Piemontese, A. Reis-Kivinen, L. Kulacz, N. Borios, and C. Amatetti, "Proof of concept for spectrum sharing between terrestrial and satellite networks," in *Proc. Joint European Conference on Networks and Communications and 6G Summit (EuCNC/6G Summit)*, 2023.
- [11] E. Lagunas, S. K. Sharma, S. Maleki, S. Chatzinoas, and B. Ottersten, "Resource allocation for cognitive satellite communications with incumbent terrestrial networks," *IEEE Transactions on Cognitive Communications and Networking*, vol. 1, no. 3, pp. 305–317, 2015.
- [12] V. Icolari, D. Tarchi, A. Guidotti, and A. Vanelli-Coralli, "Genetic inspired scheduling algorithm for cognitive satellite systems," in *Proc. IEEE International Conference on Communications (ICC)*, 2016.
- [13] G. Charbit, A. Medles, P. Jose, D. Lin, X. Zhu, and I.-K. Fu, "Satellite and cellular networks integration - a system overview," in *Proc. Joint European Conference on Networks and Communications and 6G Summit (EuCNC/6G Summit)*, 2021.
- [14] E. N. Gilbert, "Random plane networks," *Journal of the Society for Industrial and Applied Mathematics*, vol. 9, no. 4, p. 533–543, Dec. 1961.
- [15] D. Cao, S. Zhou, and Z. Niu, "Optimal combination of base station densities for energy-efficient two-tier heterogeneous cellular networks," *IEEE Transactions on Wireless Communications*, vol. 12, no. 9, pp. 4350–4362, Sep. 2013.
- [16] H. S. Dhillon, R. K. Ganti, F. Baccelli, and J. G. Andrews, "Modeling and analysis of K-tier downlink heterogeneous cellular networks," *IEEE Journal on Selected Areas in Communications*, vol. 30, no. 3, pp. 550–560, Apr. 2012.
- [17] H. S. Dhillon, R. K. Ganti, and J. G. Andrews, "Load-aware modeling and analysis of heterogeneous cellular networks," *IEEE Transactions on Wireless Communications*, vol. 12, no. 4, pp. 1666–1677, April 2013.
- [18] H. ElSawy, E. Hossain, and M. Haenggi, "Stochastic geometry for modeling, analysis, and design of multi-tier and cognitive cellular wireless networks: A survey," *IEEE Communications Surveys and Tutorials*, vol. 15, no. 3, Jun. 2013.
- [19] H. Wei, N. Deng, W. Zhou, and M. Haenggi, "Approximate SIR analysis in general heterogeneous cellular networks," *IEEE Transactions on Communications*, vol. 64, no. 3, pp. 1259–1273, Mar. 2016.
- [20] C.-h. Lee and M. Haenggi, "Interference and outage in Poisson cognitive networks," *IEEE Transactions on Wireless Communications*, vol. 11, no. 4, pp. 1392–1401, Apr. 2012.
- [21] A. H. Sakr and E. Hossain, "Cognitive and energy harvesting-based D2D communication in cellular networks: Stochastic geometry modeling and analysis," *IEEE Transactions on Communications*, vol. 63, no. 5, pp. 1867–1880, May 2015.
- [22] A. Hasan and J. G. Andrews, "The guard zone in wireless ad hoc networks," *IEEE Transactions on Wireless Communications*, vol. 6, no. 3, pp. 897–906, Mar. 2007.
- [23] A. M. Hunter, J. G. Andrews, and S. Weber, "Transmission capacity of ad hoc networks with spatial diversity," *IEEE Transactions on Wireless Communications*, vol. 7, no. 12, pp. 5058–5071, Dec. 2008.
- [24] R. K. Ganti and M. Haenggi, "Interference and outage in clustered wireless ad hoc networks," *IEEE Transactions on Information Theory*, vol. 55, no. 9, pp. 4067–4086, Sep. 2009.
- [25] F. Baccelli, B. Blaszczyszyn, and P. Muhlethaler, "Stochastic analysis of spatial and opportunistic aloha," *IEEE Journal on Selected Areas in Communications*, vol. 27, no. 7, pp. 1105–1119, Sep. 2009.
- [26] V. V. Chetlur and H. S. Dhillon, "On the load distribution of vehicular users modeled by a poisson line cox process," *IEEE Wireless Communications Letters*, vol. 9, no. 12, pp. 2121–2125, Dec. 2020.
- [27] J. P. Jeyaraj and M. Haenggi, "Cox models for vehicular networks: SIR performance and equivalence," *IEEE Transactions on Wireless Communications*, vol. 20, no. 1, pp. 171–185, Jan. 2021.
- [28] J. G. Andrews, F. Baccelli, and R. K. Ganti, "A tractable approach to coverage and rate in cellular networks," *IEEE Transactions on Communications*, vol. 59, no. 11, pp. 3122–3134, Nov. 2011.
- [29] Z. Pan and Q. Zhu, "Modeling and analysis of coverage in 3-D cellular networks," *IEEE Communications Letters*, vol. 19, no. 5, pp. 831–834, May 2015.
- [30] V. V. Chetlur and H. S. Dhillon, "Downlink coverage analysis for a finite 3-D wireless network of unmanned aerial vehicles," *IEEE Transactions on Communications*, vol. 65, no. 10, pp. 4543–4558, Oct. 2017.
- [31] X. Wang, H. Zhang, Y. Tian, and V. C. M. Leung, "Modeling and analysis of aerial base station-assisted cellular networks in finite areas under LoS and NLoS propagation," *IEEE Transactions on Wireless Communications*, vol. 17, no. 10, pp. 6985–7000, Oct. 2018.
- [32] M. M. Azari, G. Geraci, A. Garcia-Rodriguez, and S. Pollin, "UAV-to-UAV communications in cellular networks," *IEEE Transactions on Wireless Communications*, vol. 19, no. 9, pp. 6130–6144, 2020.
- [33] O. Y. Kolawole, S. Vuppala, M. Sellathurai, and T. Ratnarajah, "On the performance of cognitive satellite-terrestrial networks," *IEEE Transactions on Cognitive Communications and Networking*, vol. 3, no. 4, pp. 668–683, Dec. 2017.
- [34] N. Okati, T. Riihonen, D. Korpi, I. Angervuori, and R. Wichman, "Downlink Coverage and Rate Analysis of Low Earth Orbit Satellite Constellations Using Stochastic Geometry," *IEEE Transactions on Communications*, vol. 68, no. 8, pp. 5120–5134, Aug. 2020.
- [35] N. Okati and T. Riihonen, "Stochastic Analysis of Satellite Broadband by Mega-Constellations with Inclined LEOs," in *Proc. IEEE 31st Annual International Symposium on Personal, Indoor and Mobile Radio Communications (PIMRC)*, Sep. 2020.
- [36] A. Talgat, M. A. Kishk, and M.-S. Alouini, "Stochastic geometry-based analysis of LEO satellite communication systems," *IEEE Communications Letters*, Oct. 2020.
- [37] —, "Nearest neighbor and contact distance distribution for binomial point process on spherical surfaces," *IEEE Communications Letters*, vol. 24, no. 12, pp. 2659–2663, Dec. 2020.
- [38] N. Okati and T. Riihonen, "Nonhomogeneous stochastic geometry analysis of massive LEO communication constellations," *IEEE Transactions on Communications*, vol. 70, no. 3, pp. 1848–1860, Jan. 2022.
- [39] N. Okati and T. Riihonen, "Modeling and Analysis of LEO Mega-Constellations as Nonhomogeneous Poisson Point Processes," in *Proc. IEEE 93rd Vehicular Technology Conference (VTC)*, Apr. 2021.
- [40] —, "Coverage and Rate Analysis of Mega-Constellations Under Generalized Serving Satellite Selection," in *Proc. IEEE Wireless Communications and Networking Conference (WCNC)*, Apr. 2022.
- [41] —, "Stochastic coverage analysis for multi-altitude LEO satellite networks," *IEEE Communications Letters*, vol. 27, no. 12, pp. 3305–3309, Oct. 2023.
- [42] M. Afshang and H. S. Dhillon, "Fundamentals of modeling finite wireless networks using binomial point process," *IEEE Transactions on Wireless Communications*, vol. 16, no. 5, pp. 3355–3370, 2017.
- [43] "Solutions for NR to support non-terrestrial networks (NTN)," *3GPP TR38.863*, Sep. 2022.
- [44] "Satellite and terrestrial network convergence," *MediaTek 6G Technology White Paper*, 2023.
- [45] A. G. Bole, A. Wall, and A. Norris, *Radar and ARPA Manual: Radar, AIS and Target Tracking for Marine Radar Users, chapter 2*. Butterworth-Heinemann, 2013.
- [46] M. Di Renzo, "Stochastic geometry modeling and analysis of multi-tier millimeter wave cellular networks," *IEEE Transactions on Wireless Communications*, vol. 14, no. 9, pp. 5038–5057, May 2015.
- [47] S. Singh, M. N. Kulkarni, A. Ghosh, and J. G. Andrews, "Tractable model for rate in self-backhauled millimeter wave cellular networks," *IEEE Journal on Selected Areas in Communications*, vol. 33, no. 10, pp. 2196–2211, May 2015.
- [48] "Study on International Mobile Telecommunications (IMT) parameters for 6.425 - 7.025 GHz, 7.025 - 7.125 GHz and 10.0 - 10.5 GHz," *3GPP TR138.921*, Sep. 2022.
- [49] T. S. Rappaport, *Wireless communications: Principles and practice*. Pearson Education India, 2010.